PKA catalytic subunits dissociate from regulatory subunits to regulate neuronal functions

Wei-Hong Xiong[a], Maozhen Qin[a], and Haining Zhong[a,1]

a. Vollum Institute, Oregon Health & Science University, Portland, OR 97239, USA

1. Correspondence should be addressed to H.Z. (email: zhong@ohsu.edu).

Haining Zhong, Ph.D.
Vollum Institute, Oregon Health & Science University
3181 SW Sam Jackson Park Road, L474
Portland, Oregon 97239
U.S.A.
(503) 494-5089 / zhong@ohsu.edu

Key words: cAMP-dependent kinase / protein kinase A (PKA); two-photon imaging; norepinephrine; shRNA knockdown; late-phase structural long-term potentiation; AMPA and NMDA-mediated synaptic transmission.

Abstract

Protein kinase A (PKA) plays essential roles in diverse cellular functions. However, the spatiotemporal dynamics of endogenous PKA upon activation remain debated. The classical model predicts that PKA catalytic subunits dissociate from regulatory subunits in the presence of cAMP, whereas a second model proposes that catalytic subunits remain associated with regulatory subunits following physiological activation. Here we report that different PKA subtypes, as defined by the regulatory subunit, exhibit distinct subcellular localization at rest in CA1 neurons of cultured hippocampal slices. Nevertheless, when all tested PKA subtypes are activated via the β-adrenergic receptor by norepinephrine, catalytic subunits translocate to dendritic spines but regulatory subunits remain unmoved. These differential spatial dynamics between the subunits indicate that at least a significant fraction of PKA dissociates. Furthermore, PKA-dependent regulation of synaptic plasticity and transmission can be supported only by wildtype, dissociable PKA, but not by non-dissociable PKA. These results argue for the classical model in which endogenous PKA regulatory and catalytic subunits dissociate to achieve PKA function.

31 **Significance**

32 Protein kinase A (PKA) is the major effector of the second messenger cAMP and plays a
33 critical role in numerous cell biology processes. The function and specificity of PKA rely on
34 spatial compartmentalization. However, the precise subcellular distribution and dynamics
35 of activated PKA remain debated. Textbooks illustrate that upon activation PKA catalytic
36 subunits dissociate from regulatory subunits. However, some recent work has proposed
37 that PKA catalytic subunits remain associated with regulatory subunits following
38 physiological activation. The present study tests these two models in the context of
39 neuronal function. The results support the classical model of PKA activation. A clarified
40 model of PKA action will contribute to the understanding of how the specificity of PKA
41 phosphorylation may be achieved.

42

43 **INTRODUCTION**

44 Cyclic adenosine monophosphate (cAMP)-dependent kinase, or protein kinase A (PKA),
45 regulates diverse critical functions in nearly all mammalian cells. PKA is a tetrameric
46 protein consisting of two regulatory subunits (PKA-Rs) and two catalytic subunits (PKA-Cs)
47 (1, 2). In the inactive state, each PKA-R binds to and inhibits a PKA-C. Binding of cAMP to
48 PKA-R activates PKA-C. However, there are different proposals on the molecular events
49 that follow activation.

50 For decades, PKA-C is thought to dissociate from PKA-R upon cAMP binding. Freed
51 PKA-C molecules then move to phosphorylate their substrates. However, two recent
52 studies propose an alternative model, in which physiological concentrations of cAMP can
53 activate PKA-C but do not result in its dissociation from PKA-R (3, 4). Testing these two
54 models will not only elucidate the biophysical mechanism of PKA activation, but also have
55 distinct implications in how PKA may achieve its specificity, which is thought to rely on
56 spatial compartmentalization (5).

57 We have previously found that the majority of type IIβ PKA, as defined by PKA-R, is
58 anchored to microtubules in the dendritic shaft of hippocampal CA1 pyramidal neurons
59 where PKA-RIIβ is bound to the abundant microtubule associated protein MAP-2 (6). Upon
60 activation of the β-adrenergic receptor with norepinephrine, a fraction of PKA-C
61 dissociated from PKA-RIIβ (7). The freed PKA-C redistributed into dendritic spines,
62 whereas PKA-RIIβ remained anchored at the dendritic shaft (7, 8). These results are
63 consistent with the classical PKA activation model. However, recent studies suggest that
64 PKA-Rs other than PKA-RIIβ may be the more abundant isoforms in CA1 neurons (9, 10). It

65 remains unknown whether these PKA isoforms dissociate upon physiologically relevant
66 stimulations.

67 Here, we examined whether PKA-C dissociates from the major PKA-R isoforms,
68 PKA-RIβ and PKA-RIIα, in CA1 neurons. The rescue of function following knockdown of
69 PKA-C was examined using wildtype dissociable PKA versus a non-dissociable PKA variant
70 in which PKA-C is covalently linked to PKA-R. The result supports the classical model of
71 PKA activation via dissociation.

72 **Results**

73 Recent studies have suggested that PKA-RIIα and PKA-RIβ may be the prevalent
74 isoforms in hippocampal CA1 neurons. Therefore, we co-expressed EGFP tagged PKA-C
75 (PKA-C-EGFP) and a cytosolic marker (mCherry) with either PKA-RIIα or PKA-RIβ in CA1
76 neurons of organotypic hippocampal slice cultures (Figs. 1A and 1B, upper left panels).
77 PKA-C-EGFP exhibited a resting distribution that was dependent on the co-expressed PKA-
78 R: when co-expressed with PKA-RIIα, PKA-C was enriched in dendritic shafts; when co-
79 expressed with PKA-Riβ, PKA-C was more evenly distributed (quantified using the spine
80 enrichment indexes, or SEI, see Methods) (Fig. 1C). This distribution largely mimicked that
81 of the corresponding PKA-R (Figs. 1A-1C).

82 Notably, upon application of norepinephrine (10 μM), PKA-C of both subtypes
83 translocated to dendritic spines, but the subcellular localization of PKA-Rs remained
84 unchanged (Figs. 1D & 1E). This differential re-distribution between PKA-C and PKA-R was
85 more prominent following activation with forskolin (25 μM) and IBMX (50 μM). These
86 results can only be explained if at least a fraction of PKA-C dissociated from both PKA-RIIα

87 and PKA-RIβ when a physiological stimulant was used. Together with our earlier results
88 regarding PKA-C/PKA-RIIβ, we conclude that PKA-C dissociates from PKA-R with
89 physiologically relevant stimuli.

90 Next, we asked whether PKA regulation of neuronal function is dependent on the
91 dissociation of PKA-C from PKA-R. A key experiment supporting the non-dissociating PKA
92 activation model was that PKA regulation of cell growth could be sustained by a construct
93 in which PKA-C was fused to PKA-RIIα in one polypeptide chain via a flexible linker (named
94 R-C; Fig. 1F). We therefore asked whether this R-C construct could support PKA regulation
95 of neuronal function. When R-C-EGFP was expressed in CA1 neurons, this construct
96 exhibited a distribution highly similar to that of RIIα at the resting state (Fig. 1G and 1H).
97 The tendency of this construct to translocate to the spine was largely diminished compared
98 to PKA-C-EGFP co-expressed with wildtype, unlinked PKA-RIIα (Fig. 1I).

99 To determine the function of R-C, a previously established shRNA construct was
100 used to selectively knock down PKA-Cα in CA1 neurons in cultured hippocampal slices (7).
101 Given that PKA activation is required for the late phase of long-term potentiation (L-LTP)
102 (11), we examined the structural LTP of individual dendritic spines of CA1 neurons elicited
103 by focal two-photon glutamate uncaging (Figs. 2A–2C) (12). The shRNA knockdown of
104 PKA-C resulted in attenuated LTP at around 90 min after induction (Figs. 2A–2C). This
105 attenuation was not observed when a control shRNA against LacZ was expressed (Fig. 2C).
106 The attenuated structural LTP was rescued by co-expression of shRNA-resistant wild-type
107 PKA-C-EGFP together with PKA-RIIα (Figs. 2A–2C). However, the R-C construct in which

108 PKA-C was also resistant to shRNA knockdown but could not leave PKA-RIIα failed to
109 rescue the phenotype.

110 PKA activity has also been shown to regulate synaptic transmission. We therefore
111 examined evoked AMPA and NMDA receptor (AMPAR and NMDAR, respectively) currents
112 in paired, transfected and adjacent untransfected CA1 neurons in cultured hippocampal
113 slices. As shown previously (7), neurons expressing the shRNA construct against PKA-C
114 exhibited significantly lower AMPAR currents (Fig. 2D), but not NMDAR currents (Fig. 2E).
115 As a result, the AMPAR/NMDAR current ratio was also reduced (Fig. 2F). The reduced
116 AMPAR currents and reduced AMAPR/NMDAR current ratios were rescued by co-
117 expression of shRNA-resistant, wild-type dissociable PKA-C-EGFP and PKA-RIIα (Figs. 2D–
118 2F). However, the non-dissociable R-C construct failed to rescue the phenotype. Taken
119 together, the R-C construct did not support normal PKA-dependent synaptic function.

120 **Discussion**

121 The results indicate that at least a fraction of PKA-C molecules dissociate from all
122 tested PKA-R isoforms when activated by physiological stimuli. Given that PKA activity
123 increases by two orders of magnitude when dissociated from PKA-R (13), even a small
124 fraction of PKA-C dissociation will result in a marked increase of PKA kinase activity.
125 Notably, our results corroborate the recent results in HEK cells that used biochemical
126 measurements to show that PKA-C and PKA-R indeed dissociate in intact cells (14).
127 Furthermore, the PKA-C that is covalently linked to PKA-RIIα cannot functionally replace
128 wildtype PKA for normal neuronal transmission or plasticity. Although the R-C construct
129 has been shown to functionally replace endogenous PKA in terms of supporting the growth

130 of a heterologous cell line (4), our results indicate that it cannot support all necessary PKA
131 functions. Overall, we conclude that PKA-C dissociation from PKA-R is essential for PKA
132 regulation of neuronal function. Additionally, PKA specificity is mediated by spatial
133 compartmentalization (5). This is likely mediated by mechanism downstream of PKA
134 dissociation, such as membrane tethering of freed PKA-C or its buffering by extra PKA-Rs
135 (7, 14).

136 This study also demonstrates that PKA is essential for long-term structural LTP of
137 individual spines. PKA has been shown to facilitate the induction of LTP (i.e.,
138 metaplasticity) (15), and is required for the maintenance of L-LTP (11), as assayed using
139 electrophysiological recording of postsynaptic currents. However, it has been suggested
140 that the structural and synaptic current changes may not be causal (16). Our results fill the
141 gap to show that PKA is also required for the late phase of structural LTP.

142

143 **Materials and Methods**

144 **Plasmid constructs**

145 Constructs were made using standard mutagenesis and subcloning methods. All previously
146 unpublished constructs and their sequences will be submitted to Addgene. In the R-C
147 construct, mouse PKA-RIIα and PKA-Cα were fused via a linker with residues
148 WDPGSGSLEAGCKNFFPRSFTSCGSLEGGSAAA that were previously used (4).

149 **Organotypic hippocampal slice cultures and transfections**

150 Cultured rat hippocampal slices were prepared from P6 – P8 (typically P7) pups, as
151 described previously (6, 17). Animal experiments were performed in accordance with the
152 Guide for the Care and Use of Laboratory Animals of the National Institutes of Health, and
153 were approved by the Institutional Animal Care and Use Committee (IACUC) of the Oregon
154 Health & Science University (#IP00002274). cDNA constructs were transfected after 1.5–3
155 weeks *in vitro* via the biolistic gene transfer method using the Helios gene gun and 1.6 μm
156 gold beads (Fig. 1) or, where long-term expression (~ 1 week) was required, with single-
157 cell electroporation (Fig. 2) (18).

158 **Two-photon imaging and two-photon glutamate uncaging**

159 A custom built two-photon microscope based on an Olympus BW51WI microscope body
160 was used. Laser beams from two different Ti:Sapphire lasers (Maitai, Newport) were
161 aligned to allow for simultaneous two-photon excitation and photoactivation. Laser
162 intensities were controlled by Pockels cells (Conoptics). Imaging and photoactivation were
163 controlled by ScanImage (Vidrio Tech) (19). Slices were perfused in gassed artificial
164 cerebral spinal fluid (ACSF) containing 4 mM Ca, 4 mM Mg, and 0.5 μM tetrodotoxin (TTX)

165 during imaging. mEGFP fluorescence (green) was unmixed from that of the cytosolic
166 marker (mCherry or DsRed Express) using a dichroic (Chroma 565DCXR) and band-pass
167 filters (Chroma HQ510/70 for green and Semrock FF01-630/92 for red).

168 For single-spine structural LTP experiments, 2.25 mM MNI-caged-L-glutamate
169 (Tocris) was added to ACSF containing 4 mM calcium, 0.05 mM magnesium, 1 μM TTX and
170 4 μM 2-chloroadenosine, as previously described (20). To trigger structural plasticity, 30
171 pulses of 4-ms 16-mW (at back focal plane) 720-nm laser light were delivered to the spine
172 head at 0.5 Hz.

173 Image analysis was performed using custom software written in MATLAB called
174 *SI_View* (https://github.com/HZhongLab/SI_View) (21). Using the software, regions of
175 interest (ROIs) were manually drawn to isolate spines or their immediately adjacent
176 dendritic shaft. Only the spines well isolated from the dendrite laterally throughout the
177 entire experiments were included. Spine enrichment index was calculated as:

178 $$SEI = \log_2[(F_{green}/F_{red})_{spine}/(F_{green}/F_{red})_{shaft}]$$

179 in which F is the average fluorescence intensity in an ROI.

180 **Electrophysiology**

181 Whole-cell voltage-clamp recordings were performed using a MultiClamp 700B amplifier
182 (Molecular Devices). Electrophysiological signals were filtered at 2 kHz and digitized and
183 acquired at 20 kHz using custom software written in MATLAB. Slices were perfused with
184 artificial cerebrospinal fluid containing 4 mM Ca and 4 mM Mg. The internal solution
185 contained (in mM) 132 Cs-gluconate, 10 HEPES, 10 Na-phosphocreatine, 4 MgCl2, 4 Na2-

186 ATP, 0.4 Na-GTP, 3 Na-ascorbate, 3 QX314, and 0.2 EGTA with an osmolarity of 295
187 mOsmol/kg. The junction potential was calculated to be -17 mV using a built-in function in
188 the Clampfit software (Molecular Devices). Several less abundant anions (phosphocreatine,
189 ATP, GTP and ascorbate) were omitted in the calculation due to lack of data in the program.
190 The Cl reversal potential was -75 mV.

191 To reduce recurrent activities, cultured hippocampal slices were cut on both sides of
192 CA1 and 4 μM 2-chloroadenosine (Sigma) was present in all recording experiments. 10 μM
193 GABAzine (SR 95531, Tocris) was also included to suppress GABA currents. For electrical
194 stimulation, a bipolar, θ-glass stimulating electrode (Warner Instruments) was positioned
195 in the stratum radiatum 100–150 μm lateral to the recorded neuron. For all recordings, a
196 transfected neuron and an untransfected neuron located within 50 μm of each other were
197 sequentially recorded without repositioning the stimulation electrode. Measurements were
198 carried out on averaged traces from approximately 20 trials under each condition. For
199 AMPAR currents, the cells were held at -60 mV (before correcting for the junction
200 potential) and the current was measured as the baseline-subtracted peak current within a
201 window of 2–50 ms after electric stimulation. For NMDAR currents, the average currents at
202 140 to 160 ms after stimulation were used when the cells were held at +55 mV (before
203 correcting for the junction potential)

204 **Data analysis, presentation, and statistics**

205 Quantification and statistical tests were performed using custom software written in
206 MATLAB. Averaged data are presented as mean ± s.e.m., unless noted otherwise. p values
207 were obtained from one-way ANOVA tests, unless noted otherwise. In all figures, *: $p \leq 0.05$

208 and is considered statistically significant after Bonferroni correction for multiple tests, **: $p \leq 0.01$, and ***: $p \leq 0.001$.

Acknowledgements

We thank all members of the Mao and Zhong laboratories at the Vollum Institute for constructive discussions. We thank Drs John Williams and Michael Muniak for critical comments and edits on the manuscript. This work was supported by two NIH BRAIN Initiative awards to H.Z. (U01NS094247 and R01NS127013).

Author contributions

H.Z. conceived the project. W.X. and H.Z. designed the experiments. W.X. and H.Z. performed the experiments and data analyses. M.Q. produced critical reagents used in the experiments. H.Z. wrote the manuscript.

Competing interests

The authors declare no competing interests.

223 **References**

224 1. S. H. Francis, J. D. Corbin, Structure and Function of Cyclic Nucleotide-Dependent
225 Protein Kinases. *Annu. Rev. Physiol.* (1994)
226 https:/doi.org/10.1146/annurev.ph.56.030194.001321.

227 2. D. A. Johnson, P. Akamine, E. Radzio-Andzelm, Madhusudan, S. S. Taylor, Dynamics of
228 cAMP-dependent protein kinase. *Chem. Rev.* (2001)
229 https:/doi.org/10.1021/cr000226k.

230 3. F. D. Smith, *et al.*, Intrinsic disorder within an AKAP-protein kinase A complex guides
231 local substrate phosphorylation. *Elife* **2013** (2013).

232 4. F. D. Smith, *et al.*, Local protein kinase A action proceeds through intact holoenzymes.
233 *Science (80-.).* **356** (2017).

234 5. W. Wong, J. D. Scott, AKAP signalling complexes: Focal points in space and time. *Nat.*
235 *Rev. Mol. Cell Biol.* (2004) https:/doi.org/10.1038/nrm1527.

236 6. H. Zhong, *et al.*, Subcellular Dynamics of Type II PKA in Neurons. *Neuron* **62**, 363–374
237 (2009).

238 7. S. E. Tillo, *et al.*, Liberated PKA Catalytic Subunits Associate with the Membrane via
239 Myristoylation to Preferentially Phosphorylate Membrane Substrates. *Cell Rep.* **19**,
240 617–629 (2017).

241 8. W. H. Xiong, M. Qin, H. Zhong, Myristoylation alone is sufficient for PKA catalytic
242 subunits to associate with the plasma membrane to regulate neuronal functions.

243 *Proc. Natl. Acad. Sci. U. S. A.* **118** (2021).

244 9. M. Weisenhaus, *et al.*, Mutations in AKAP5 disrupt dendritic signaling complexes and
245 lead to electrophysiological and behavioral phenotypes in mice. *PLoS One* **5** (2010).

246 10. R. Ilouz, *et al.*, Isoform-specific subcellular localization and function of protein kinase
247 a identified by mosaic imaging of mouse brain. *Elife* **6** (2017).

248 11. T. Abel, *et al.*, Genetic demonstration of a role for PKA in the late phase of LTP and in
249 hippocampus-based long-term memory. *Cell* **88**, 615–626 (1997).

250 12. M. Matsuzaki, N. Honkura, G. C. R. Ellis-Davies, H. Kasai, Structural basis of long-term
251 potentiation in single dendritic spines. *Nature* **429**, 761–766 (2004).

252 13. E. Miyamoto, J. F. Kuo, P. Greengard, Cyclic nucleotide-dependent protein kinases. 3.
253 Purification and properties of adenosine 3',5'-monophosphate-dependent protein
254 kinase from bovine brain. *J. Biol. Chem.* **244** (1969).

255 14. R. Walker-Gray, F. Stengel, M. G. Gold, Mechanisms for restraining cAMP-dependent
256 protein kinase revealed by subunit quantitation and cross-linking approaches. *Proc.*
257 *Natl. Acad. Sci. U. S. A.* **114** (2017).

258 15. M. J. Thomas, T. D. Moody, M. Makhinson, T. J. O'Dell, Activity-dependent β-
259 adrenergic modulation of low frequency stimulation induced LTP in the hippocampal
260 CA1 region. *Neuron* **17**, 475–482 (1996).

261 16. C. D. Kopec, B. Li, W. Wei, J. Boehm, R. Malinow, Glutamate receptor exocytosis and
262 spine enlargement during chemically induced long-term potentiation. *J. Neurosci.* **26**

263 (2006).

264 17. L. Stoppini, P. A. Buchs, D. Muller, A simple method for organotypic cultures of
265 nervous tissue. *J. Neurosci. Methods* (1991) https:/doi.org/10.1016/0165-
266 0270(91)90128-M.

267 18. N. Otmakhov, J. Lisman, Measuring CaMKII concentration in dendritic spines. *J.*
268 *Neurosci. Methods* (2012) https:/doi.org/10.1016/j.jneumeth.2011.09.022.

269 19. T. A. Pologruto, B. L. Sabatini, K. Svoboda, ScanImage: Flexible software for operating
270 laser scanning microscopes. *Biomed. Eng. Online* **2**, 13 (2003).

271 20. C. D. Harvey, R. Yasuda, H. Zhong, K. Svoboda, The spread of Ras activity triggered by
272 activation of a single dendritic spine. *Science (80-.).* **321**, 136–140 (2008).

273 21. L. Ma, *et al.*, Locomotion activates PKA through dopamine and adenosine in striatal
274 neurons. *Nature* **611**, 762–768 (2022).

275

276 **Figure legends**

277 **Fig. 1.** PKA-C but not PKA-R or a non-dissociable R-C redistribute to spines upon
278 activation. (*A*, *B*) Representative two-photon images of PKA-C-EGFP co-expressed with
279 PKA-RIIα or PKA-RIβ at rest, or in the presence of norepinephrine (NE) or forskolin and
280 IBMX (F + I). mCherry (magenta) was co-expressed to reveal the neuronal morphology. (*C*–
281 *E*) Quantification and comparison of the spine enrichment index at the resting state (C) and
282 upon activation (*D* & *E*). As in panel *C* from left to right, n (spines/neurons) = 53/11, 34/7,
283 33/6, and 36/7. (*F*) Schematic of wildtype PKA versus R-C. In both cases PKA-C was tagged
284 by mEGFP. (*G*–*I*) Representative images (*G*), quantifications of resting distribution (*H*), and
285 the distribution change upon stimulation by forskolin and IBMX (*I*) of R-C compared to
286 PKA-RIIα-EGFP and co-expressed PKA-C-EGFP/PKA-RIIα. n (spines/neurons) = 48/10.

287 **Fig. 2.** PKA regulation of synaptic plasticity and synaptic transmission cannot be sustained
288 using a non-dissociable PKA variant. (*A*–*C*) Representative image (*A*), time course (*B*), and
289 the degree of potentiation (*C*) at the indicated timepoints in panel *B* of single-spine LTP
290 experiments as triggered by focal glutamate uncaging at the marked spines (gray dot). In
291 panel *B*, both stimulated spines (solid circles) and non-stimulated control spines (open
292 circles) are shown. As in panel *C* from left to right, n (spines, each from a different neuron)
293 = 8, 7, 17, 11, 9. (*D*–*F*) Representative traces (red) normalized to the paired control (blue)
294 (insets) and scatter plots of paired AMPA (*D*) and NMDA (*E*) receptor currents and
295 AMPA/NMDA receptor current ratios (*F*) from neighboring untransfected CA1 neurons
296 paired with those transfected with shRNA against PKA-C and the indicated shRNA-resistant

297 rescue constructs. Statistical p values were obtained using a sign test (MATLAB). From left

298 to right, n (neuron pairs) = 13, 11, 11, and 15.

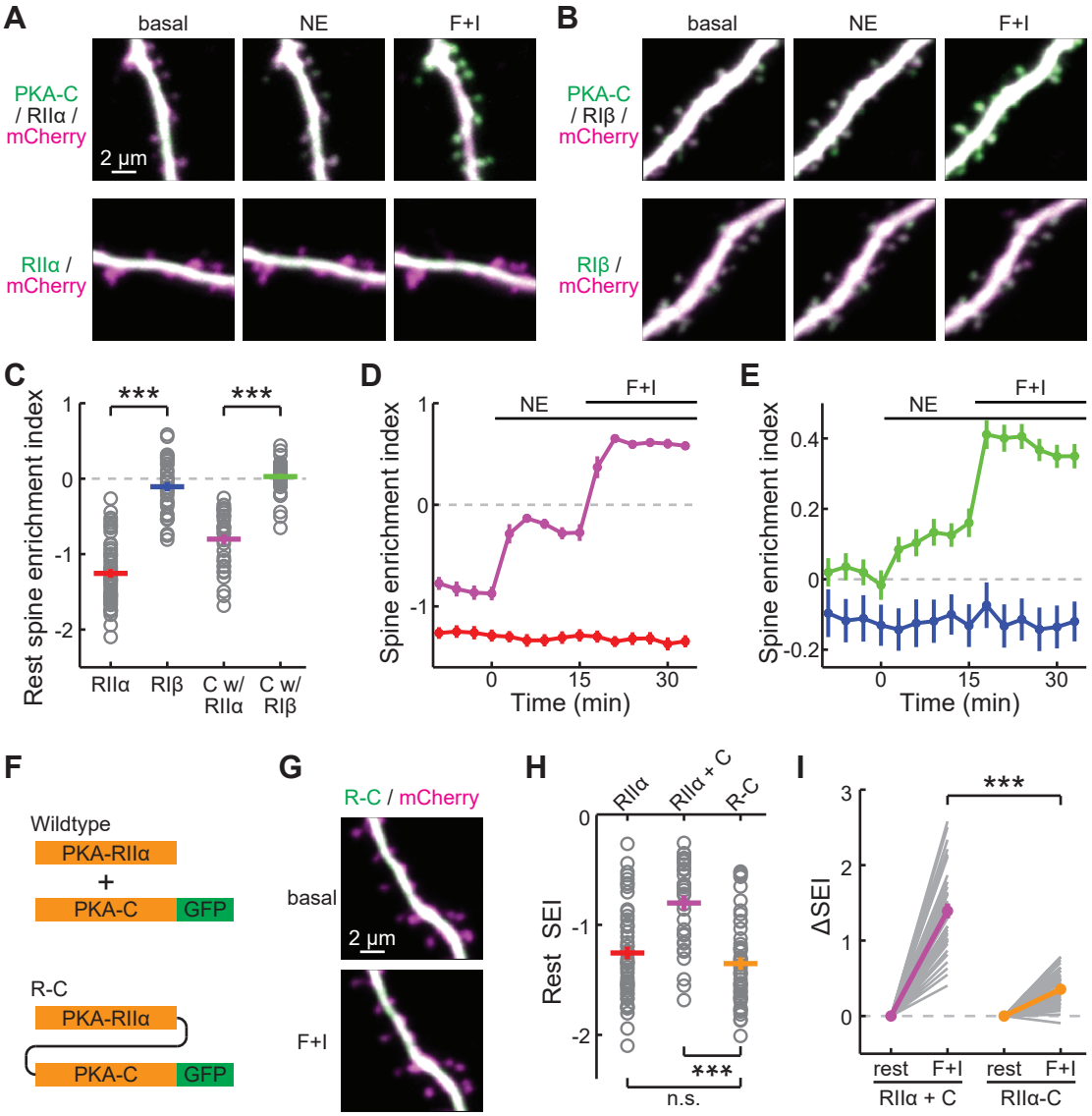

Xiong et al._Figure 1

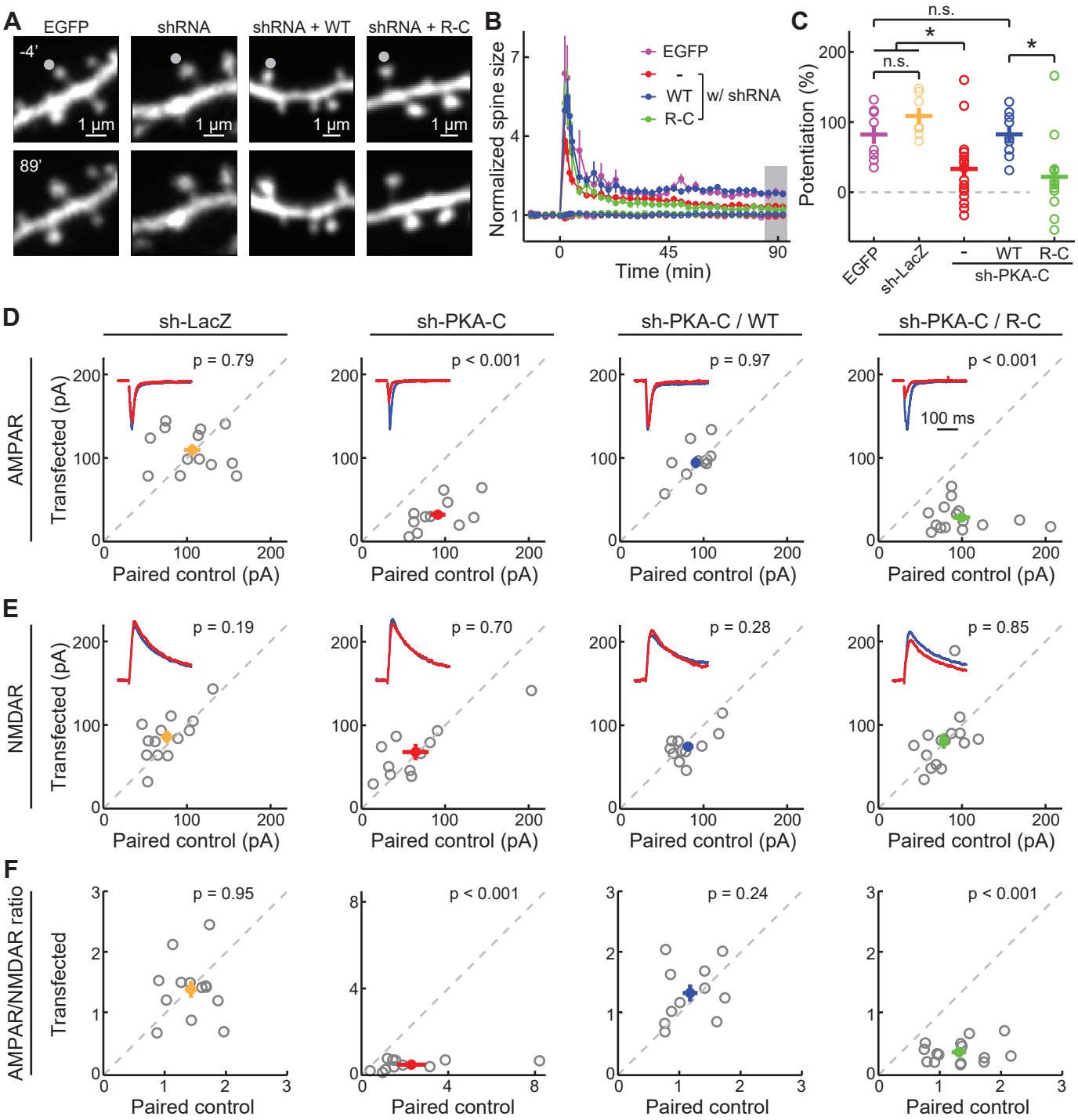

Xiong et al._Figure 2